Anal. Chem. **2004,** *76,* 1633−1640

Multiparameter Microscopy and Spectroscopy for Single-Molecule Analytics

Michael Prummer,*,†,‡ Beate Sick,‡,§ Alois Renn,|| and Urs P. Wild||

Institute of Biomolecular Sciences, Swiss Federal Institute of Technology Lausanne (EPFL), Lausanne, Switzerland, DNA Array Facility, Center for Integrative Genomics, University of Lausanne, Lausanne, Switzerland, and Physical Chemistry Laboratory, Swiss Federal Institute of Technology Zürich (ETHZ), Zürich, Switzerland

The ability to monitor several parameters simultaneously from distinct individual fluorescent reporter molecules facilitates the disentanglement of complex and interacting systems and opens new perspectives in areas from basic science to biopharmaceutical technology. By combining annular illumination microscopy, time-correlated single-photon counting, and multichannel detection, we were able to determine 14 independent parameters from one individual fluorophore. The whole set of parameters was deduced from the few properties of the fluorescence photons, i.e., arrival time, wavelength, and polarization. With this approach, the intensity, the polarization, and the spectral dynamics can be analyzed on a nanosecond time scale and the mean values can be monitored with submillisecond time resolution. Nanosecond spectral dynamics of single molecules has been observed, to the best of our knowledge, for the first time. From our experience, we can determine all parameters for more than 30% of the illuminated fluorophores in biological samples and for more than 80% in doped polymeric films.

One of the smallest available sensing device one can think of is a single molecule reporting on the state of its nanoenvironment by the emission of light. Consequently, spatial heterogeneities in the vicinity of the fluorophore can be revealed on a molecular scale. By monitoring single molecules, thus avoiding ensemble averaging, even uncorrelated dynamical processes that are hidden in conventional experimental approaches become accessible.

So far, single molecules have been utilized as nanoscopic sensing devices in various situations to detect local concentrations of different substances, such as ATP,[1,2] O_2,[3,4] H^+,[5] or Na^+,[6] to name only a few. Furthermore, they allow for monitoring a variety of (bio)chemical reactions, among many others, ligand−receptor binding in low concentration colocalization assays, while excluding false positive events due to unspecific adsorption.[7]

Because of the multiple interactions of single fluorophores with their environment, sets of simultaneously determined different parameters are ideally suited to sense several material characteristics and dynamical processes in parallel. When the systems under investigation become more complex, more parameters need to be determined with appropriate accuracy to draw unambiguous conclusions.

For example, in a major publication by Rothwell et al.,[8] the authors used single-molecule fluorescence resonance energy transfer (FRET) and a multiparameter fluorescence detection technique to reveal structurally distinct complexes of reverse transcriptase/DNA complexes, which were not observed by X-ray crystallography. Global analysis of donor lifetime, spectral ratio, and anisotropy was employed to distinguish real FRET events from side effects, like quenching or spectral jumps, and to resolve the different subpopulations, which are difficult to distinguish otherwise.

Another work was presented recently by Vallee et al.,[9] where nanoscale density fluctuations in polymers were studied using a single-molecule probe. The observed asymmetric lifetime variations of the probe could be attributed to local density changes of the surrounding polymer matrix, after alternative interpretations were ruled out. This was achieved by comparing the trajectories of intensity and lifetime, which were simultaneously obtained from the same probe molecule.

In modern analytic applications, such as high-throughput and high-content screening, a high reliability has to be achieved after a low number of detected photons. In a previous paper, we could show that the single-molecule identification efficiency can be increased by a factor of 10 when, in addition to a lifetime discrimination procedure, a separation in two spectral channels is applied.[10] Hence, the number of photons necessary to distinguish one dye molecule out of four species with 99.9% accuracy

* Corresponding author: Michael.Prummer@epfl.ch.
† EPFL.
‡ Both authors contributed equally to the work.
§ University of Lausanne.
|| ETHZ.

(1) Schnitzer, M. J.; Block, S. M. *Nature* **1997**, *388*, 386-390.
(2) Ishijima, A.; Kojima, H.; Funatsu, T.; Tokunaga, M.; Higuchi, H.; Tanaka, H.; Yanagida, T. *Cell* **1998**, *92*, 161−171.
(3) Veerman, J. A.; Garcia-Parajo, M. F.; Kuipers, L.; van Hulst, N. F. *Phys. Rev. Lett.* **1999**, *83*, 2155−2158.
(4) Hübner, C. G.; Renn, A.; Renge, I.; Wild, U. P. *J. Chem. Phys.* **2001**, *115*, 9619−9622.
(5) Brasselet, S.; Moerner, W. E. *Single Mol.* **2000**, *1*, 17−23.
(6) Kaim, G.; Prummer, M.; Sick, B.; Zumofen, G.; Renn, A.; Wild, U. P.; Dimroth, P. *FEBS Lett.* **2002**, *525*, 156−163.
(7) Schütz, G. J.; Trabesinger, W.; Schmidt, T. *Biophys. J.* **1998**, *74*, 2223−2226.
(8) Rothwell, P. J.; Berger, S.; Kensch, O.; Felekyan, S.; Antonik, M.; Wöhrl, B. M.; Restle, T.; Goody, R. S.; Seidel, C. A. *Proc. Natl. Acad. Sci. U.S.A.* **2003**, *100*, 1655−1660.
(9) Vallee R. A.; Tomczak N.; Kuipers L.; Vancso G. J.; Van Hulst N. F. *Phys. Rev. Lett.* **2003**, *91*, 038301.
(10) Prummer, M.; Hübner, C. G.; Sick, B.; Hecht, B.; Renn, A.; Wild, U. P. *Anal. Chem.* **2000**, *72*, 443−447.

10.1021/ac034976g CCC: $27.50
Published on Web 02/07/2004

is reduced to a few hundred, which is a precondition, for example, for efficient single-molecule DNA sequencing.

Despite the undisputable benefit of the analysis of multiple quantities, in previous studies, only a comparably low number of parameters has been determined simultaneously of one and the same molecule. So far, the fluorescence lifetime has been recorded together with spectral information[10] and both as a function of time.[11] Lifetimes have further been investigated in conjunction with intensity[12,13] and with orientation.[14] Time courses of emission spectra[15,16] as well as singlet−triplet transition kinetics[3,4] have been recorded.

In this paper, we want to demonstrate the current state of multiparameter single-molecule fluorescence experiments and determine a large number of parameters simultaneously from one individual molecule. All direct observables are carried by the fluorescence photons, i.e., polarization, wavelength, absolute detection time, and arrival time after pulsed excitation. In the following, we describe the determination of 14 parameters of one single fluorophore from these observables. Subsequently, we evaluate the applicability of these measurements by estimating the fractions of molecules for which different sets of parameters can be determined with appropriate precision, depending on the number of detected photons before photobleaching.

The discussed parameters are generally independent from each other in the sense that none of them can be derived from the others. Nevertheless, in several experimental situations, some of them are strongly coupled. Measuring combinations of these parameters simultaneously for one and the same molecule therefore allows for the correlation of different quantities. This ability is especially helpful in exploratory research, where one generally has no complete a priori knowledge about the expected experimental outcome.

Beyond those parameters that have already been determined separately before, we performed nanosecond time-resolved spectral ratiometry to the best of our knowledge for the first time on single molecules.

EXPERIMENTAL SECTION

Polymer films containing isolated fluorescent molecules were prepared by spin-casting (9600 rpm) a solution of poly(methyl methacrylate) (PMMA; Fluka 81359) in toluene (10 μL, 0.07 wt %) onto standard glass coverslips. The solution contained 0.1 nM dioctadecyltetramethylindocarbocyanine (DiI(C_{18}); Molecular Probes D-282) or the perylene derivative J51. Coverslips were precleaned by baking at 500 °C for 2 h. The difference between the refractive index of PMMA (1.48) and glass (1.42) is negligible. Atomic force microscopy of the polymer films near a scratch revealed a smooth surface and a film thickness of ∼30 nm.

Dye-labeled protein samples were prepared as described:[17,18] A single-cysteine mutant of the citrate transport protein CitS was labeled specifically with a single Alexa546−maleimide (Molecular Probes A-10258). The detergent-solubilized protein−dye complex was immobilized via its poly-His-tag on an NTA-functionalized coverslip by Ni^{2+}−chelate complex formation. The experiments were performed immediately after the addition of CitS (2 μL, 30 nM) to the buffer (60 μL, 50 mM K_2HPO_4, 100 mM KCl, 0.05% DDM, pH 7.0).

An outline of the experimental setup used in this study is shown in Figure 1, and a detailed description is posted as Supporting Information. A pulsed Nd:YAG laser at 532 nm is focused by a 1.4 NA oil immersion objective to a diffraction-limited spot on the sample plane. For orientational imaging, a circular annular aperture can be placed into the center of the excitation beam. Images are acquired by raster scanning the sample through the focus and collecting the photons at each pixel. After appropriate filtering, the emission light is detected by three avalanche photodiodes (APDs): APD1 detects the vertical polarization component. The horizontal component is further split by a dichroic mirror into a short-wavelength part (APD2) and a long-wavelength part (APD3). The pulses from the APDs are routed to a time-correlating single photon counting (TCSPC) computer board, where the arrival time after the excitation pulse, the absolute time, and the number of the detector are stored for each photon.

Data analysis, especially least-squares fitting, and presentation was entirely performed with Igor Pro (Wavemetrics).

RESULTS AND DISCUSSION

Single-Molecule Microscopy. A sketch of the custom-designed multiparameter microscope is presented in Figure 1. The essential features are as follows: (i) pulsed laser excitation, (ii) annular illumination, and (iii) multichannel detection. With a TCSPC computer board, the arrival time after pulsed excitation, the detection time, and the channel number are stored for each photon. This type of data acquisition allows for a flexible analysis of the time, polarization, and spectrally resolved fluorescence emission of single molecules. Images are recorded point by point by scanning the sample through a diffraction-limited focal spot with nanometer precision.

From a scanning image (Figure 2) the intensity and the two-dimensional (2D) lateral (x,y) position are obtained. This is achieved by fitting a 2D Gaussian to the image data. The full width at half-maximum (fwhm) of the point spread function (probed with a single fluorophore excited at 532 nm) was determined to be 208 ± 2 nm and represents the optical resolution of this confocal microscope. This is very close to the theoretical limit (195 nm), taking into account the excitation wavelength, the numerical aperture of the objective, and the detection pinhole size, which is in our case determined by the active area of the detector. With a total of ∼50 000 collected photons per spot, the position can be determined with an accuracy of 1 nm and a reproducibility better than 5 nm as a result of the mechanical stability of the instrument. With this precision, super-resolution distance measurements are possible,[19] which can be exploited to determine colocalization events in low-concentration binding assays.

(11) Tinnefeld, P.; Herten, D. P.; Sauer, M. *J. Phys. Chem. A* **2001**, *105*, 7989−8003.
(12) Van Orden, A.; Machara, N. P.; Goodwin, P. M.; Keller, R. A. *Anal. Chem.* **1998**, *70*, 1444−1451.
(13) Palo, K.; Brand, L.; Eggeling, C.; Jäger, S.; Kask, P.; Gall, K. *Biophys. J.* **2002**, *83*, 605−618.
(14) Kreiter, M.; Prummer, M.; Hecht, B.; Wild, U. P. *J. Chem. Phys.* **2002**, *117*, 9430−9433.
(15) Lu, H. P.; Xie, X. S. *Nature* **1997**, 385, 143−146.
(16) Blum, C.; Stracke, F.; Becker, S.; Müllen, K.; Meixner, A. J. *J. Phys. Chem. A* **2001**, *105*, 6983−6990.
(17) Kästner, C. N.; Dimroth, P.; Pos, K. M. *Arch. Microbiol.* **2000**, *174*, 67−73.
(18) Kästner, C. N.; Prummer, M.; Sick, B.; Renn, A.; Wild, U. P.; Dimroth, P. *Biophys. J.* **2003**, *84*, 1651−1659.
(19) Lacoste, T. D.; Michalet, X.; Pinaud, F.; Chemla, D. S.; Alivisatos, A. P.; Weiss, S. *Proc. Natl. Acad. Sci. U.S.A.* **2000**, *97*, 9461−9466.

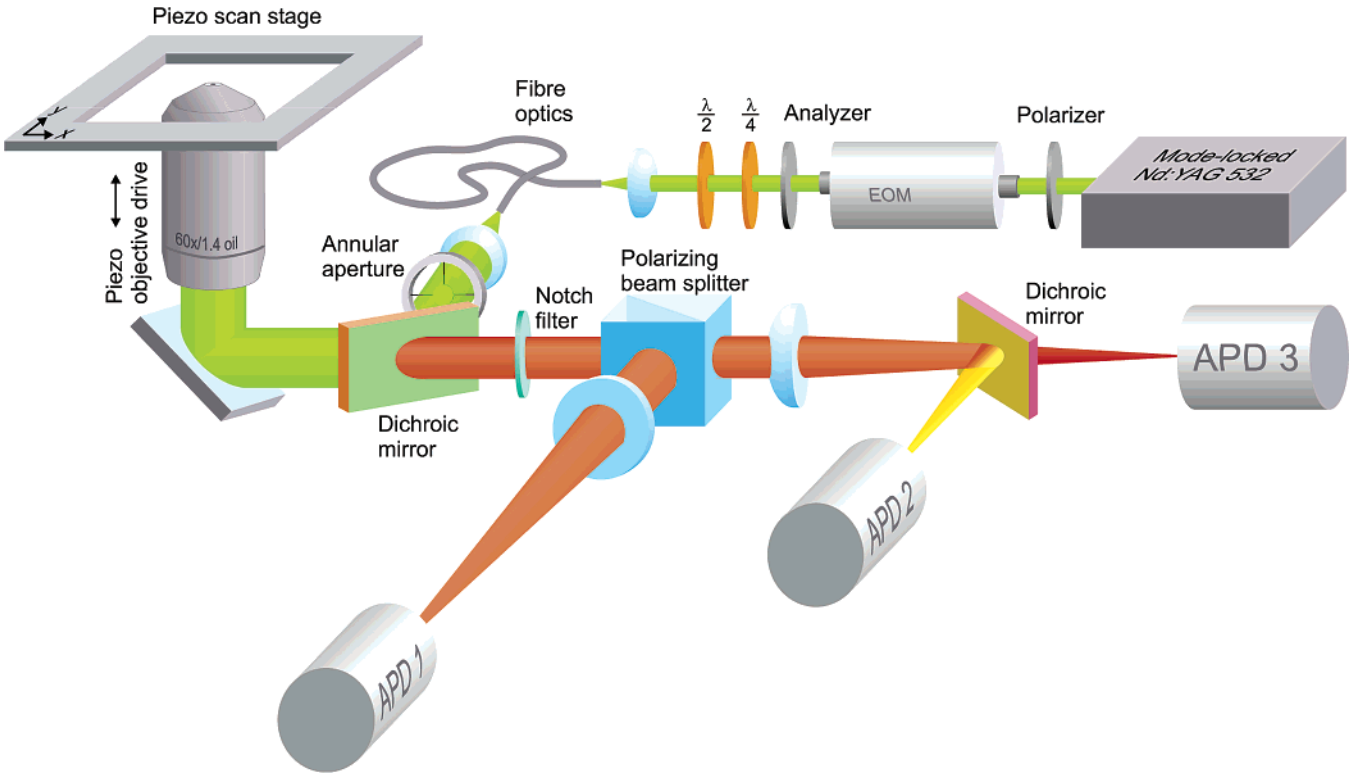

Figure 1. Optical setup of the confocal microscope for single-molecule multiparameter microscopy/spectroscopy. The instrument comprises pulsed laser excitation, annular illumination, and multichannel detection. A detailed description is given in the Experimental Section and as Supporting Information.

Orientational Imaging. A new method for orientational imaging was recently developed in our group,[20,21] which relies on the fact that a fluorescent molecule interacts with an optical field via its absorption dipole moment. For excitation intensities far from saturation the fluorescence rate $R(\vec{r})$ of a single molecule located at $\vec{r}$ is given by

$$R(\vec{r}) = c|\ \hat{d}\cdot\vec{E}(\vec{r})|^2 \qquad (1)$$

where $\hat{d}$ is the unit vector along the absorption dipole moment of the molecule, $\vec{E}(\vec{r})$ is the electric field vector at the position of the molecule, and c is a constant. Accordingly, by scanning a single fluorophore within the focal plane, the image pattern of the fluorophore, which is detected point by point, is a nanometer-scale map of the squared electrical field component parallel to the molecular absorption dipole.

For the excitation of single molecules of arbitrary orientation, we engineered a focal field distribution with components of comparable magnitudes in all directions by using annular illumination through a high numerical aperture objective lens on a polymer/air interface.[20,21] Panels a and b of Figure 3 show two fluorescence scanning images of DiI in PMMA recorded successively from the same area with vertically and horizontally polarized incident light, respectively. The different patterns show characteristic single-molecule properties: some of the patterns are truncated at the top side because of digital photobleaching during line-by-line image acquisition, and some patterns exhibit intermittent dark spots due to excursions of the dye molecule to the triplet state.

By comparing the measured image patterns of a single fluorophore with calculated distributions of the squared electric field components[20,21,14] the three-dimensional (3D) orientation of the molecular absorption dipole is determined (Figure 3c). The best fit yields an in-plane angle $\phi = -15.5°$ and an out-of-plane angle $\beta = -34°$. An error analysis of the fitting procedure revealed an accuracy of better than 5°.[14] Both successively recorded patterns are consistent with the same orientation, indicating a rigid fixation of the dye molecule within the polymer matrix. Not only the 3D orientation but also the lateral 2D position of molecule A can be extracted from the images in Figure 3. All the remaining parameters are determined for the same molecule A, if not stated otherwise.

Fluorescence Dynamics. After the aperture was removed from the excitation path, molecule A was illuminated continuously with linearly polarized light at increased excitation intensity while the emitted photons were collected by three detectors (shown in Figure 1). The total emission intensity is calculated from a stream of photons with a relatively high time resolution of 50 μs/time bin (Figure 4). The laser is switched on shortly after 0.25 s, and the molecule bleaches just after 0.55 s. The magnification (inset) shows two discrete intensity levels, light periods and dark periods.

During a light period, the molecule cycles between the ground and the excited singlet state, whereas during the dark periods, it dwells in the triplet state. The number of cycles in the light period prior to an excursion to the triplet state characterizes the

(20) Sick, B.; Hecht, B.; Novotny, L. *Phys. Rev. Lett.* **2000**, *85*, 4482−4485.
(21) Sick, B.; Hecht, B.; Wild, U. P.; Novotny, L. *J. Microsc. (Oxford)* **2001**, *202*, 365−373.

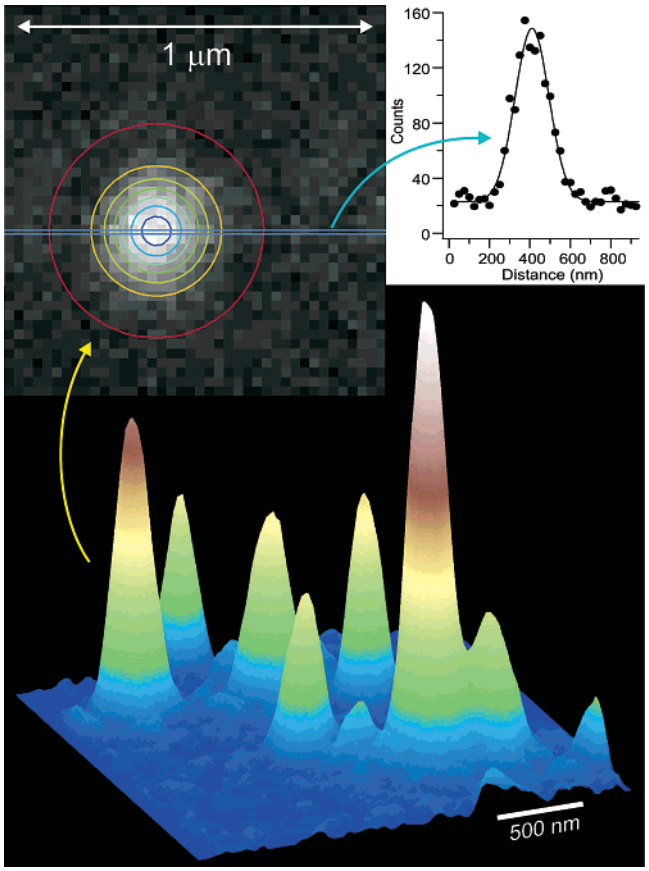

Figure 2. Surface profile of a filtered scanning image of isolated fluorophores (J51/PMMA). The maximum amplitude corresponds to 200 counts. Top left: raw data of the indicated molecule in gray scale together with a Gaussian best fit as a contour plot. Top right: Line cut of the left image taken along the blue line with an fwhm of 208 nm.

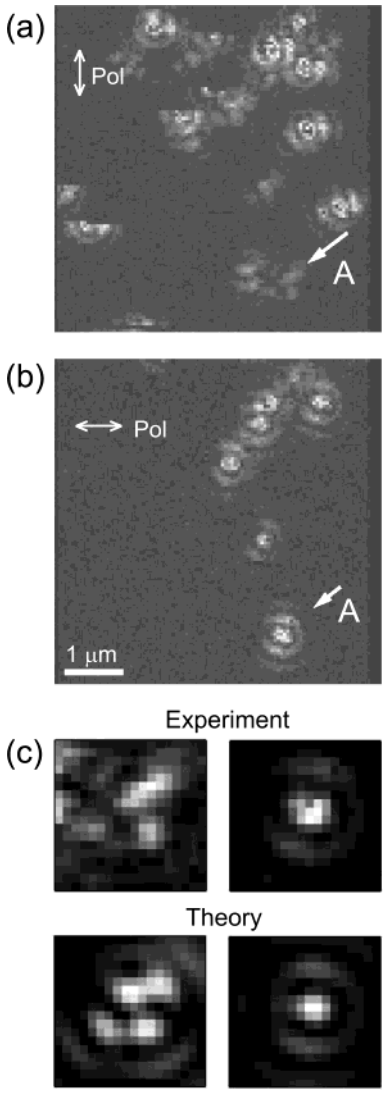

Figure 3. Confocal orientational imaging. Images of DiI in PMMA with annular illumination and (a) vertical and (b) horizontal excitation polarization recorded successively from the same area. The 14 parameters are determined for molecule A at the bottom right (arrow). (c) Comparison of the experimentally obtained intensity patterns with patterns calculated from the theoretical field distribution. The in-plane angle is −15.5°; the out-of-plane angle is −34.0°.

intersystem crossing yield Y_{ISC}. Accordingly, Y_{ISC} can be extracted from a histogram of the number of photons in each on-time (Figure 5a). An exponential fit yields $Y_{ISC} = (4.9 \pm 0.5) \times 10^{-4}$, assuming a detection efficiency of $10 \pm 2\%$, well within the average for DiI in PMMA.[3,4]

From the distribution of the dark period durations of molecule A, the triplet lifetime $\tau_T = 380 \pm 30\ \mu s$ is obtained (Figure 5b). From the distribution of arrival times, the fluorescence lifetime is derived (Figure 5c) by an exponential fit to be $\tau_F = 2.33 \pm 0.03$ ns, with symmetrically distributed residuals.

Exploiting the information obtained with a multichannel detection scheme (Figure 1), we can determine the spectral ratio r_S (eq 2), the polarization P (eq 3), and the anisotropy A (eq 4) of the emitted fluorescence light:

$$r_S = (I_3 - I_2)/(I_3 + I_2) \quad (2)$$

$$P = (I_1 - (I_2 + I_3))/(I_1 + (I_2 + I_3)) \quad (3)$$

$$A = (I_{||} - I_\perp)/(I_{||} + 2I_\perp) \quad (4)$$

where I_3 is the long-wavelength and I_2 is the short-wavelength component with respect to the corner wavelength of the dichroic mirror; I_1 is vertically and $(I_2 + I_3)$ is horizontally polarized (see Figure 1). $I_{||}$ is the detected intensity with polarization parallel to the excitation light, and $I_\perp$ is polarized perpendicularly.

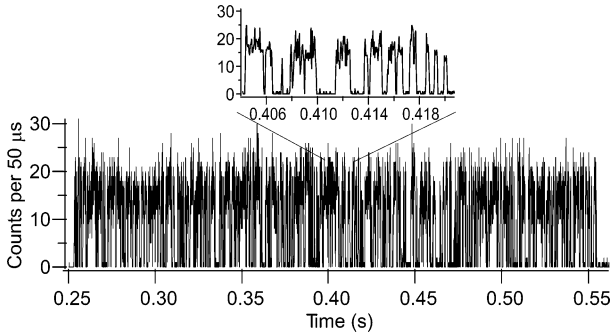

Figure 4. Intensity time series of molecule A. The high time resolution allows for the determination of on-times, when the molecules cycles between ground and excited state, and off-times, when it stays in the triplet state (inset).

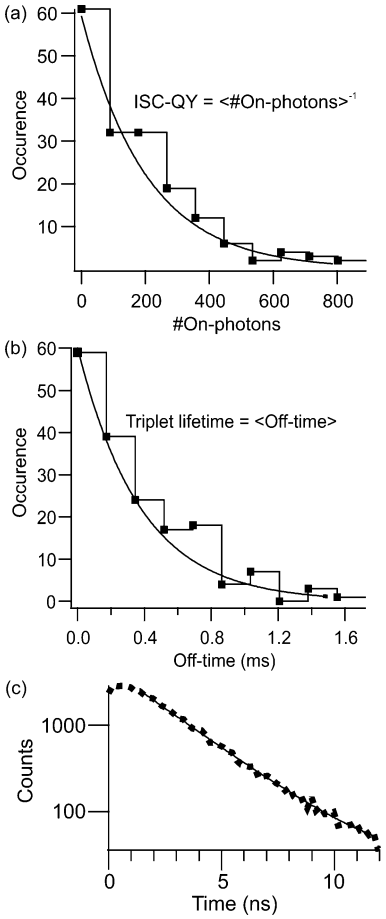

Figure 5. Analysis of the fluorescence dynamics. (a) Histogram of the number of photons during an on-time, (b) histogram of the off-time durations, and (c) histogram of the arrival times. From the fitted single exponentials, the intersystem crossing yield ($Y_{ISC} = (4.9 \pm 0.5) \times 10^{-4}$, assuming a detection efficiency of 10%), the triplet lifetime ($\tau_T = 380 \pm 30\ \mu$s), and the singlet lifetime ($\tau_F = 2.33 \pm 0.03$ ns) are determined.

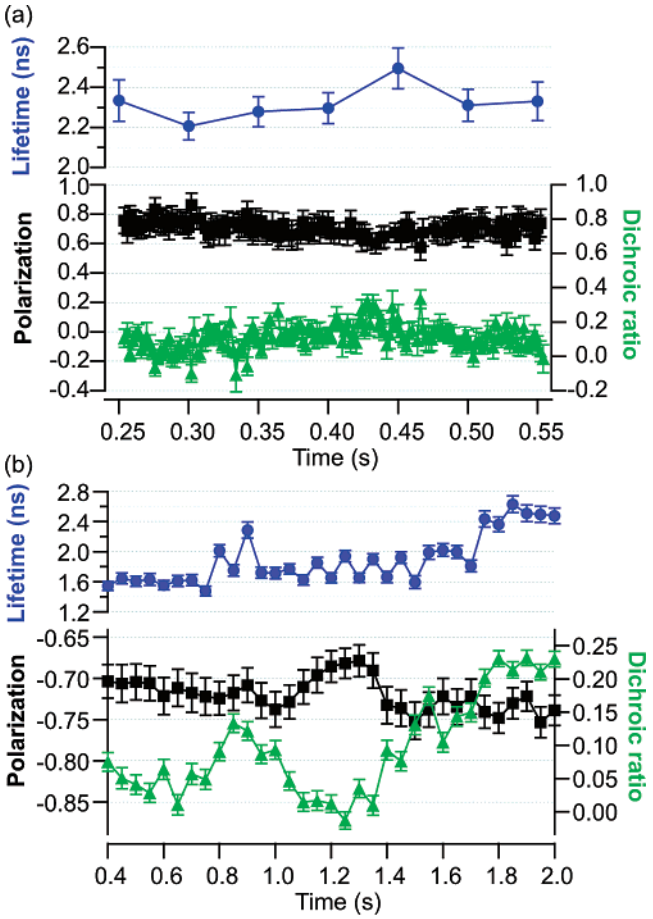

Figure 6. Time-resolved measurement of the fluorescence lifetime (blue circles, upper panel), the steady-state emission polarization (black sqares), and the spectral ratio (green triangles) for molecule A (a), and another DiI molecule from the same sample (b). Error bars represent one standard deviation.

Relying on the fact that the radiation of most fluorophores is linearly polarized along the molecular emission dipole, we can utilize the polarization (eq 3) and the anisotropy (eq 4) to follow orientational changes of the fluorophore. Analogously, changes in the spectral ratio (eq 2) indicate spectral dynamics.

Due to the high signal strength and the fact that in the experiment all information is stored on a photon-by-photon basis, the time traces of fluorescence lifetime, polarization, and spectral ratio can be determined with (sub)millisecond resolution. Figure 6 shows the three time series in this order from top to bottom. The error bars in the lifetime traces are obtained from the nonlinear least-squares algorithm. The remaining error bars are computed via error propagation from the shot noise in each detector. For molecule A, the polarization and the spectral ratio are constant on this millisecond time scale (Figure 6a). The fluorescence lifetime on the other hand shows significant variations from 2.2 to 2.5 ns. Although the origin of these variations is unknown, they may well reflect changes in the fluorophore's nanoenvironment. Figure 6b shows another example from a DiI molecule exhibiting stronger variations in all three quantities.

We determine the in-plane angle φ of the emission dipole of molecule A from the measured constant polarization $P = \cos(2\varphi) = 0.78$ as $\varphi = \pm(19 \pm 4°)$, compared to 15° of the absorption dipole. To remove the sign ambiguity and fully determine the in-plane projection of the emission dipole, the magnitude of a third projection is required, e.g., in 45° to the horizontal and vertical polarization direction.

There is evidence in the literature that the absorption and the emission dipole of DiI are not collinear. Based on an ensemble experiment of DiI in lipid membranes, a deviation of 28° has been suggested.[22] In a single-molecule near-field study of DiI in PMMA, a discrepancy of the orientation of absorption and emission dipole of at least 18° has been observed.[23] Both studies are in concordance with our results.

Time-Resolved Anisotropy. We have performed a time-resolved analysis of the anisotropy with subnanosecond resolution based on the arrival times of horizontally and vertically polarized fluorescence photons. For an isotropic ensemble the anisotropy at time $t = 0$, A_0, is given by

(22) Axelrod, D. *Biophys. J.* **1979**, *26*, 557−573.
(23) Veerman, J. A.; Garcia-Parajo, M. F.; Kuipers, L.; Van Hulst, N. F. *J. Microsc. (Oxford)* **1999**, *194*, 477−482.

$$A_0 = (3\cos^2\alpha - 1)/5 \qquad (5)$$

where α is the angle between the absorption and the emission dipole.[24,25] The anisotropy cannot exceed 0.4 in ensemble experiments due to the angular selection of a whole distribution of dipole moments. Opposed to that, a single immobilized molecule can have $A_0 = 1$ if $\alpha = 0$ (see eq 4). However, when high numerical aperture objectives are used to collect the emitted light, small perpendicular components are introduced upon refraction.[26] As a consequence, the accessible anisotropy is always slightly smaller than 1 even for a single molecule with both transition dipoles oriented parallel to the excitation polarization.

In the case of molecule A, the anisotropy remains constant within the given time window (Figure 7 inset). This result is consistent with the obtained pattern from annular illumination (Figure 3), which predicts a rotational mobility of less than 5°. On a picosecond time scale there could still exist a small amplitude wobbling motion (<5°) which would result in a reduced A_0. But there are other DiI molecules showing a significant anisotropy decay on a nanosecond time scale (Figure 7).

This behavior indicates hindered rotational dynamics, which can be modeled by the "wobbling-in-a-cone" model.[24,27] The general solution of an arbitrarily shaped body rotating in an anisotropic potential is very complex and requires a large number of parameters. To adjust the analysis to the simple structure of the data, we approximate the dye molecule with a rod-shaped body with its transition dipole moments along the axis of symmetry. If this particle is wobbling in a cone, then the anisotropy reads[24,27]

$$A = A_\infty\left\{1 + \left[\left(\frac{2}{\cos\vartheta(1+\cos\vartheta)}\right)^2 - 1\right]e^{-t/\tau_r}\right\} \qquad (6)$$

where τ_r is the rotational correlation time, A_∞ is the final anisotropy, and ϑ is the semiangle of the cone. The cone angle gives information about the rotational degree of freedom of DiI within the PMMA matrix. The decay time is inversely proportional to the rotational diffusion coefficient, which depends on the local viscosity of the medium and on the size of the rotating body (dye plus solvation shell). A fit of eq 6 yields $A_\infty = 0.683 \pm 0.003$, $\vartheta = 12.4 \pm 0.3°$, and $\tau_r = 2.7 \pm 0.4$ ns.

From the rotational correlation time τ_r, we can estimate an effective local viscosity of the polymer matrix in the vicinity of the DiI molecule. This *effective viscosity* is a result of the forces between the matrix and the dye molecule and describes the damping of the rotation of the probe molecule. It can deviate substantially from the bulk value in heterogeneous materials such as polymer networks. Calculating the viscosity from the rotational diffusion coefficient of an arbitrarily shaped body would exceed the scope of this article. Nevertheless, to give an order of magnitude estimation of the viscose damping, we approximate

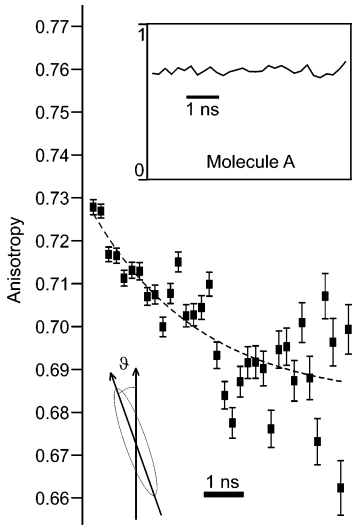

Figure 7. Time-resolved measurement of the polarization anisotropy of a single DiI molecule embedded in a polymer matrix. The dye molecule exhibits a limited rotational degree of freedom with a correlation time in the nanosecond range. Fitting yields the final anisotropy $A_\infty = 0.683 \pm 0.003$, a cone angle of wobbling ϑ of 12.4 $\pm$ 0.3°, and a rotational correlation time τ_r of 2.7 $\pm$ 0.4 ns. Inset: constant anisotropy of molecule A.

the dye by an effective cylinder of length $L = 14$ Å and radius $a = 2.5$ Å. Then $\eta = 18kT\tau_r(\ln p - 0.33)/4Vp^2 = 0.016$ Pa s, where $p = L/2a$, kT is the thermal energy, and V the approximated molecular volume.[28] This value is ~16 times the viscosity of water at room temperature.

Time-Resolved Spectral Ratiometry. The spectral shift between the absorption maximum and the emission maximum of fluorescent molecules is caused by the interactions of the fluorophore with its environment. Because of the variety of different interactions, no universal theory exists to describe the magnitude and especially the time dependence of the solvent shift.[25]

Spectrally resolved recording of the fluorescence photons by TCSPC allows for the analysis of the spectral dynamics of a fluorophore on a nanosecond time scale. For this purpose, it is convenient to choose a characteristic wavelength to describe the evolution of the spectrum with time.[29] One obvious possibility is the expectation value $\langle\lambda\rangle$ of the distribution of λ, given by the normalized emission spectrum $\hat{S}_{em}$:

$$\langle\lambda(t)\rangle = \lambda_C(t) = \int_0^\infty \lambda'\hat{S}_{em}(\lambda', t)\,d\lambda' \qquad (7)$$

$$\hat{S}_{em}(\lambda, t) = \frac{I_{em}(\lambda, t)}{\int_0^\infty I_{em}(\lambda', t)\,d\lambda'} \qquad (8)$$

The expectation value $\langle\lambda\rangle$ corresponds to the center wavelength λ_C, which splits the integral of the emission spectrum into two equal areas.

(24) Steiner, R. F. In *Topics in Fluorescence Spectroscopy*; Lakowicz, J. R., Ed.; Plenum Press: New York, 1991; Vol. 2.
(25) Lakowicz, J. R. *Principle of Fluorescence Spectroscopy*, 2 ed.; Plenum Press: New York, 1999.
(26) Wolf, E. *Proc. R. Soc. London, Ser. A* 1959, *253*, 349−379.
(27) Szabo, A. *J. Chem. Phys.* **1980**, *72*, 4620−4626.
(28) Tracy, M. A.; Pecora R. *Annu. Rev. Phys. Chem.* **1992**, *43*, 525−557.
(29) Maroncelli, M.; Fleming, G. R. *J. Chem. Phys.* **1987**, *86*, 6221−6239.

Table 1. Summary of the Survival Analysis for Two Different Model Systems[a]

set	description of parameters	no. of params	dye in polymer film (%)	dye-labeled protein (%)
A	(x,y) position, intensity, fluorescence lifetime, emission dipole projection, emission spectral ratio	6	99	94
B	as in (A), plus anisotropy decay time and amplitude, spectral relaxation time and amplitude	10	98	92
C	as in (B), plus intersystem crossing yield, triplet lifetime	12	90	54
D	as in (B), plus absorption dipole orientation	12	90	54
E	all parameters	14	80	32

[a] Shown are the fractions of molecules that emit a sufficiently large number of photons before photobleaching for the different number of parameters to be analyzed. The numbers are based on an exponential distribution of the total number of detected photons with mean values of 100 000 (dye in polymer film) and 20 000 (dye-labeled protein), respectively.

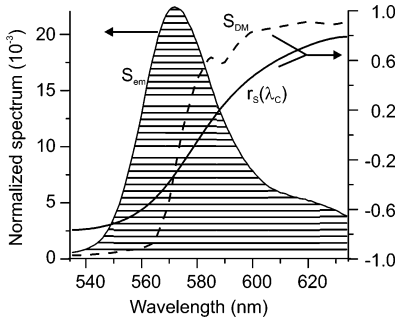

Figure 8. Spectral ratio as a function of the center wavelength (—) computed from the dichroic mirror spectrum (- - -) and the normalized emission spectrum of the dye (striped area).

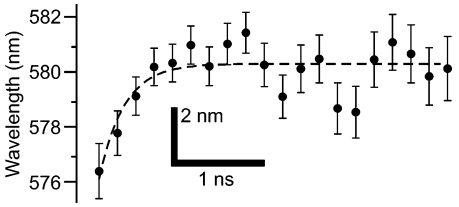

Figure 9. Time-dependent spectral relaxation of Alexa546 conjugated to a single protein. Fitting of a first-order relaxation model yields the steady-state emission wavelength $\lambda_\infty = 580$ nm, the spectral shift $\Delta\lambda = 4$ nm, and the relaxation time $\tau_\lambda = 0.3$ ns.

The spectral ratio r_S (eq 2) for a given dichroic mirror with corner wavelength λ_D and characteristic spectrumis equal to the

$$S_{DM}(\lambda;\lambda_D) = \frac{I_{trans}(\lambda;\lambda_D) - I_{refl}(\lambda;\lambda_D)}{I_{trans}(\lambda;\lambda_D) + I_{refl}(\lambda;\lambda_D)} \quad (9)$$

integral of $S_{DM}(\lambda;\lambda_D)\hat{S}_{em}(\lambda, t;\lambda_C(t))$ (Figure 8):

$$r_S(t;\lambda_C(t),\lambda_D) = \int_0^\infty S_{DM}(\lambda';\lambda_D)\hat{S}_{em}(\lambda', t;\lambda_C(t))\, d\lambda' \quad (10)$$

The inverse of this function can be used to determine the center wavelength $\lambda_C(t)$ of the spectrum and its evolution in time. The spectral dependence of the quantum efficiency of the detector of less than 5% is neglected in this calculation. A temporal shift of the center wavelength corresponds to a spectral shift of the molecular emission with time and/or to a relative change of amplitudes in the two halves of the spectrum. In both cases, the reason for the change in the spectral emission characteristics is the interaction of the dye molecule with its surrounding nanoenvironment.

We apply a phenomenological model to describe the spectral shift of the center wavelength caused by a simple relaxation of the excited state of the dye. We assume that the emission spectrum and thus its center wavelength λ_C will shift exponentially according to

$$\lambda_C(t) = \lambda_C^\infty - \Delta\lambda_C e^{-t/\tau_\lambda} \quad (11)$$

Both the amplitude of the shift $\Delta\lambda_C$ and the time constant τ_λ depend on the coupling strength of the dye with its environment.

Spectral relaxation of molecule A was too fast to be resolved or only very small. Thus, the interaction of the dye with the matrix is either weak or fast, or both. In fact, we never registered spectral relaxation in any DiI in PMMA. Relaxation could be observed, however, in dyes conjugated to proteins. Figure 9 shows a representative example of the center wavelength of Alexa546 bound to a single citrate transport protein (CitS), which is immobilized on a glass surface and covered with buffer solution. Error bars are calculated from the shot noise in each detector. A similar behavior was observed with several but not all Alexa546−CitS complexes. Fitting of eq 11 to these data yields for the different individual fluorophores a time constant $\tau_\lambda \approx 0.2-0.5$ ns and a resolved amplitude $\Delta\lambda_C \approx 4-8$ nm. The steady-state wavelength $\lambda_C^\infty = 580$ nm agrees well with the value computed from the published emission spectrum (Molecular Probes).

Solvent shifts of dyes in aqueous surrounding usually take a few picoseconds. Spectral relaxation times of dyes conjugated to proteins are reported to range from 20 ps to 20 ns.[30,31] This type of relaxation is consistent with a hierarchical structure of proteins. Molecular motion of the smaller domains occurs on a faster time scale than those of the larger domains. In particular, vibrational motions typically occur on subpicosecond to picosecond time scales, larger motions, such as rotation of aromatic rings, occur on a picosecond to nanosecond time scale, and major conformational changes occur on a microsecond to second time scale. Thus, if the protein or parts of it are flexible on a nanosecond time scale, we expect time-dependent shifts in the emission spectrum of an

(30) Gafni, A.; DeToma, R. P.; Manrow, R. E.; Brand, L. *Biophys. J.* **1977**, *17*, 155−168.
(31) Lakowicz, J. R. *Photochem. Photobiol.* **2000**, *72*, 421−437.

attached dye molecule as the polypeptide chain rearranges around the new dipole moment.

A rough order of magnitude estimation of the time scale of conformational fluctuations in proteins can be given by the ratio of the viscous drag coefficient γ and the stiffness of proteins κ, $\tau_\lambda \sim (1/5)(\kappa/\gamma)$.[25] Approximate values for a flexible amino acid loop (radius $a \approx 5$ Å, $\gamma = 6\pi\eta a \approx 60$ pN s/m, $\kappa \approx 4$ pN/nm) give $\tau_\lambda = 0.5$ ns. This number is in agreement with the relaxation time found in the present study, as well as with values obtained by molecular dynamics simulations.[32]

Survival Analysis. For practical applicability of multiparameter fluorescence spectroscopy to single-molecule analytics, it is essential that a sufficiently large number of molecules emit enough photons for a complete analysis before photobleaching. In the following we therefore summarize the number of detected photons necessary to compute the different parameters with appropriate precision. These numbers then determine the fraction of molecules for which the analysis process can be completed.

Thompson and co-workers carried out an in-depth analysis of the precision of position and intensity measurements for individual fluorescent probes.[33] According to their treatment and our experimental situation, a total of 100−200 photons are sufficient to determine the intensity with 10% accuracy, depending on the amount of background noise (in our case less than 4 counts/pixel). The position accuracy can reach 10 nm after only 500 photons are detected, when an optimized pixel size is chosen. Also, the fluorescence lifetime can be determined up to 10% with as few as 500 photons (in the range of 1−5 ns). These and the following numbers are based on Monte Carlo simulations and experimental observations. The determination of the anisotropy decay time and the spectral relaxation time requires measurements with two detection channels and therefore more signal. Values obtained from less than 1000 photons get more and more unreliable. The most photon-consuming tasks are the determination of the intersystem crossing kinetics, as well as any analysis of on- and off-times, and the orientational imaging. In these cases, ~10 000 photons are required for 10% and 5° accuracy, respectively.

To demonstrate the usefulness of our method, we calculated the number of molecules that survive the analysis up to different stages for two exemplified classes: dye-doped polymer films, such as DiI in PMMA, from which a mean photon number of $\sim 10^5$ can be detected, and labeled biological samples, such as dye-labeled proteins immobilized in aqueous medium, which allow the collection of at least 20 000 photons on average. Table 1 shows the resulting fractions of molecules that allow the analysis of the indicated number of parameters, assuming that the number of emitted photons before photobleaching is exponentially distributed among different molecules. All 14 parameters can be analyzed from 80% of the fluorophores in a polymeric host and still from 32 of the biological samples. When either the absorption dipole orientation or the kinetics of the triplet state is excluded, the 12 remaining parameters can be determined simultaneously from more than 50% even in the case of dye-labeled proteins.

This analysis again demonstrates that the method presented in this article not only provides superior information content of individual molecules, allowing for their detailed classification and analysis in minute quantities, it also bears the efficiency and sensitivity for high-throughput screening applications.

CONCLUSION

In this article, we demonstrated the observation of 14 independent parameters of one individual fluorophore. Multiparameter fluorescence spectroscopy yields the position of the dye molecule (2 coordinates), the emission intensity, the absorption dipole orientation (2 angles), the in-plane emission dipole orientation (1 angle), the excited-state lifetime, the intersystem crossing yield, the triplet lifetime, the anisotropy decay time and amplitude, the spectral relaxation time, the solvent shift, and the steady-state emission wavelength. The fluorescence lifetime, the center wavelength of emission, and the polarization were monitored with submillisecond time resolution. Time-resolved spectral relaxation on a nanosecond time scale was observed for the first time at the level of single molecules.

Evaluating combinations of larger numbers of parameters will have an increasing impact in cases where ultrasensitive methods are needed, as in modern high-throughput drug discovery. Screening methods often rely on detecting binding events between target molecules and potential drugs. Binding events between labeled targets or drugs and their counterpart can have different effects revealed by different parameters, like changes of the intensity (the complex contains more labels), fluorescence lifetime (quenching), emission spectrum (FRET), and translational and rotational dynamics (changes of the size). Thus, combinations of these parameters will provide a more reliable and efficient detection of binding events. To obtain as much information as possible from the limited number of photons available from single fluorophores, it is highly desirable to measure and derive simultaneously as many parameters as possible with appropriate time resolution.

ACKNOWLEDGMENT

We are grateful to C.N. Kaestner and B. Meyer for providing the labeled His-tagged fusion proteins, to H. Langhals for his kind gift of the perylene derivative J51, and to M. Kreiter for help with the fitting routine to analyze the orientation patterns. Fruitful discussions with B. Hecht, C.G. Hübner, B. Kharlamow, R. Kühnemuth, V. Sandoghdar, and J.-M. Segura are gratefully acknowledged. This project has been funded by the ETH Zürich and the Swiss National Science Foundation (SNF).

SUPPORTING INFORMATION AVAILABLE

Additional information as noted in text. This material is available free of charge via the Internet at http://pubs.acs.org.

Received for review August 21, 2003. Accepted January 8, 2004.

AC034976G

(32) Bockmann, R. A.; Grubmüller, H. *Nat. Struct. Biol.* **2002**, *9*, 198−202.
(33) Thompson, R. E.; Larson, D. R.; Webb, W. W. *Biophys. J.* **2002**, *82*, 2775−2783.